ELSEVIER

Journal of Volcanology and Geothermal Research 94 (1999) 219–231

Journal of volcanology and geothermal research

www.elsevier.com/locate/jvolgeores

Fogo Volcano, Cape Verde Islands: seismicity-derived constraints on the mechanism of the 1995 eruption

S.I.N. Heleno da Silva [a,*], S.J. Day [b], J.F.B.D. Fonseca [a]

[a] *Instituto Superior Técnico, Departamento de Fisica, Av. Rovisco Pais 1, 1096 Lisbon Codex, Portugal*
[b] *Benfield Greig Centre for Hazard Research, UCL, UK*

Received 10 May 1999

Abstract

Seismic data recorded in the vicinity of the active vent of the 1995 Fogo eruption [Global Volcanism Network Bulletin, 1995, 20(3) 2–4.] is used to constrain the associated stress field and deformation. Using the frequency content of the seismograms to distinguish between brittle fracture of cold host rock and deformation in the vicinity of the intruding magma, a sub-vertical dyke with 060° strike is identified as the feeder of the eruption, and delineated down to a depth of about 4 km. The local stress field during the eruption is estimated from composite focal mechanisms. Besides the expected σ_3 direction normal to the dyke, a group of focal solutions point to a stress field with nearly dyke-parallel σ_3, which is interpreted as a re-adjustment of the edifice following the eruption, maybe partially controlled by gravity. This effect may have increased the instability of the steep eastern flank of the island, since the deformation detected during the magma drainback is compatible with predominantly dip-slip motion on east-dipping surfaces.

Keywords: seismicity; eruption; Fogo Volcano, Cape Verde Islands

1. Geological and volcanological setting

The topography of Fogo island is asymmetric and characterised by a collapse-related structure with a diameter of about 9 km, opening towards the East (see Day et al., 1999-this volume, for a more detailed description of the geology and volcanic structure of Fogo). Post-collapse eruptions have partially filled this depression, which at present has a ''caldera-like'' flat area at an altitude of 1700 m, called ''Chã das Caldeiras'', surrounded by a 1000-m-high collapse scarp, the ''Bordeira'', on all sides but the East. The highest point of the island is the main volcanic cone within the Chã das Caldeiras, the Pico do Fogo, reaching 2928 m (Fig. 1).

On the basis of the distribution of scoria cones, scoria cone elongation directions and the distribution of dykes in the Bordeira escarpment and in coastal cliffs, Day et al. (1999-this volume) describe several preferred directions of dyke intrusion, or volcanic rift zones, in Fogo. These are distributed radially with respect to the axis of the old (pre-collapse) volcanic edifice, the Monte Amarelo edifice defined by Day et al. (1999-this volume). The geometry of these rift zones is broadly similar to the triple-rift geometry recognized by Carracedo (1994) (see also Carracedo,

* Corresponding author. E-mail: sisilva@alfa.ist.utl.pt

0377-0273/99/$ - see front matter
PII: S0377-0273(99)00104-3

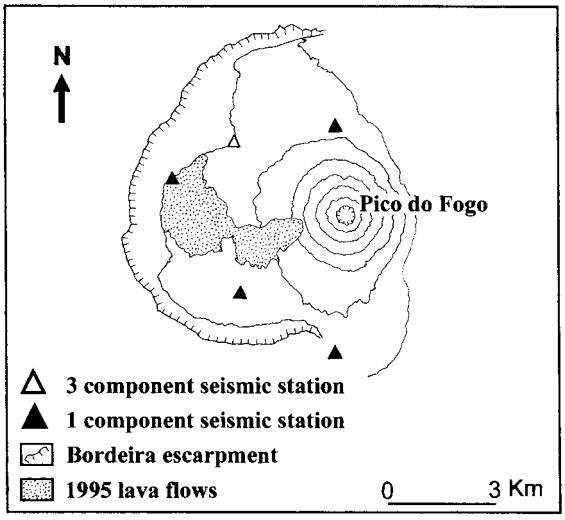

Fig. 1. Main topographic and structural aspects of Chã das Caldeiras, Fogo Island. The triangles show seismic stations deployed during the 1995 Fogo eruption. Cartographic elements after Torres et al. (1997). Contour lines are spaced 200 m.

1999-this volume) in many ocean island volcanoes, but has been slightly modified by the pre-existing structure of the Fogo–Brava platform (Day et al., 1999-this volume). The rift zones run to the NNE (bearings 000° to 030°), SSE (bearings 140° to 180°) and in a broad zone to the WSW, W and WNW of the center of the Monte Amarelo edifice. In the dyke swarms exposed in the Bordeira cliffs, in particular, this western zone appears to contain two distinct rift zones bearing 240° and 300°.

At the end of the 18th century, the earlier historic volcanic activity, characterised by frequent eruptions at the summit crater of the Pico do Fogo and by flank eruptions (Ribeiro, 1960), ceased and gave way to less frequent activity occurring solely on the lower flanks of the Pico do Fogo and on the floor of Chã das Caldeiras. These eruptions occurred at N–S elongated vents grouped in a broadly N–S elongate zone extending both north and south of the Pico do Fogo (Day et al., 1999-this volume). This geometry can be accounted for in terms of E–W extension at shallow levels within the volcano, associated with eastward gravitational sliding of the steep eastern flank of Fogo within the old collapse scar (Day et al., 1999-this volume). In the 1995 eruption, however, the orientation of the main surface vent and of the associated fumarolic zones is approximately 060°, i.e., it follows one of the broad volcanic rift zones described above, and is located at the extreme SW

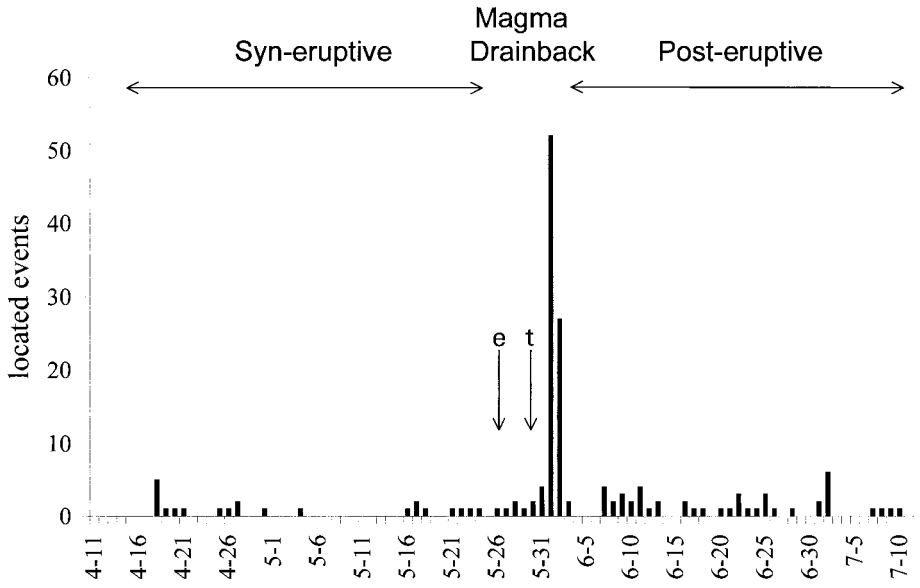

Fig. 2. Histogram with the time distribution of the seismicity recorded during the April 1995 eruption (located events only). The vertical arrows mark the end of the effusive phase (e), and the occurrence of a 45-min-long episode of strong volcanic tremor (t).

edge of the zone of post-18th century vents (Day et al., 1999-this volume). This trend, never observed in historical eruptions, is that followed by numerous young sub-historic vents, both in Chã das Caldeiras and to the WSW on the western flank of the island (Day et al., 1999-this volume).

2. Seismic data

During the April 1995 eruption of Fogo Volcano, Cape Verde Islands (Global Volcanism Network, 1995), a portable telemetered network of five seismic stations, one of which with three components, was deployed within a few kilometres of the active vent (Fonseca et al., 1996). The operation of the network started 11 days after the onset of the eruption, and the seismicity was recorded continuously for 13 weeks.

Due to equipment availability limitations and the emergency nature of the deployment, analogue recording equipment was used. To avoid the saturation of the inherent low dynamic range by the high-

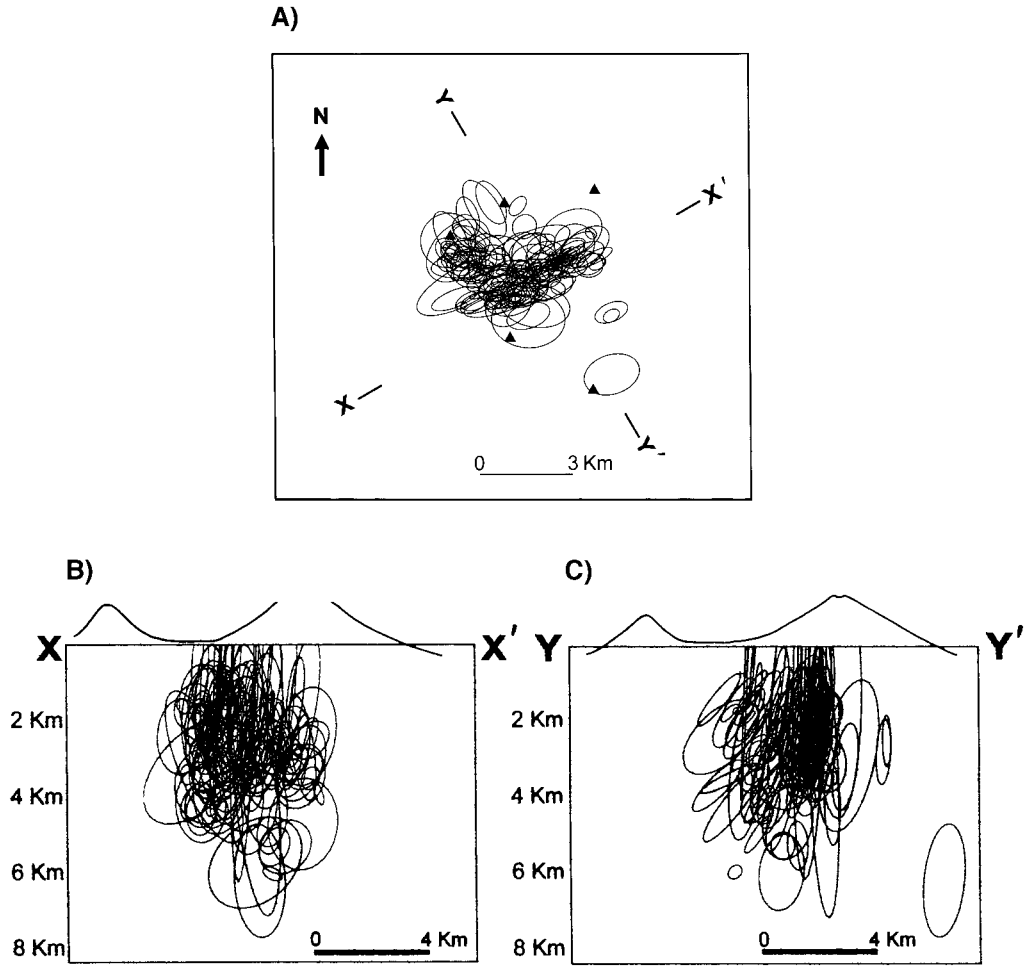

Fig. 3. (A) Epicentral distribution of the 158 seismic events located (90% confidence ellipses). Triangles show the location of seismic stations. (B) Hypocentres projected in a section parallel to the surface fissure. (C) Hypocentres projected on a section perpendicular to the surface fissure.

energy low-frequency seismic noise generated by the lava flows at short distances from the sites, geophones with natural frequency of 4.5 Hz were employed (Fonseca et al., 1996). The geometry of the network (Fig. 1) was strongly conditioned by the topography, due to the requirement of line-of-sight, and also by the access restrictions imposed by the on-going eruption. The data acquisition and processing are described in detail by Fonseca et al. (1996).

In this paper, we use results from the seismic monitoring to place constraints on the eruptive mechanism, focusing on (1) the spatial distribution of hypocentres and (2) the orientation of the stress axes inferred from composite focal mechanisms.

Over 1000 seismic events were identified and analysed for P and S phases. Of these, only 158 were located with HYPOCENTER 3.2 (Lienert, 1994), due mainly to the emergent nature of many signals and to the difficulty in identifying the S phases (using one three-component station only). Fig. 2 is a histogram of the temporal distribution of the located events. It shows three phases of seismic activity, correlating well with the field descriptions of the eruption's chronology (Gaspar et al., 1995; Torres et al., 1995). These will be referred to in the sequence as ''syn-eruptive phase'', ''magma-drainback phase'' and ''post-eruptive phase''. The first phase lasted 8 weeks, and finished at the end of the effusive activ-

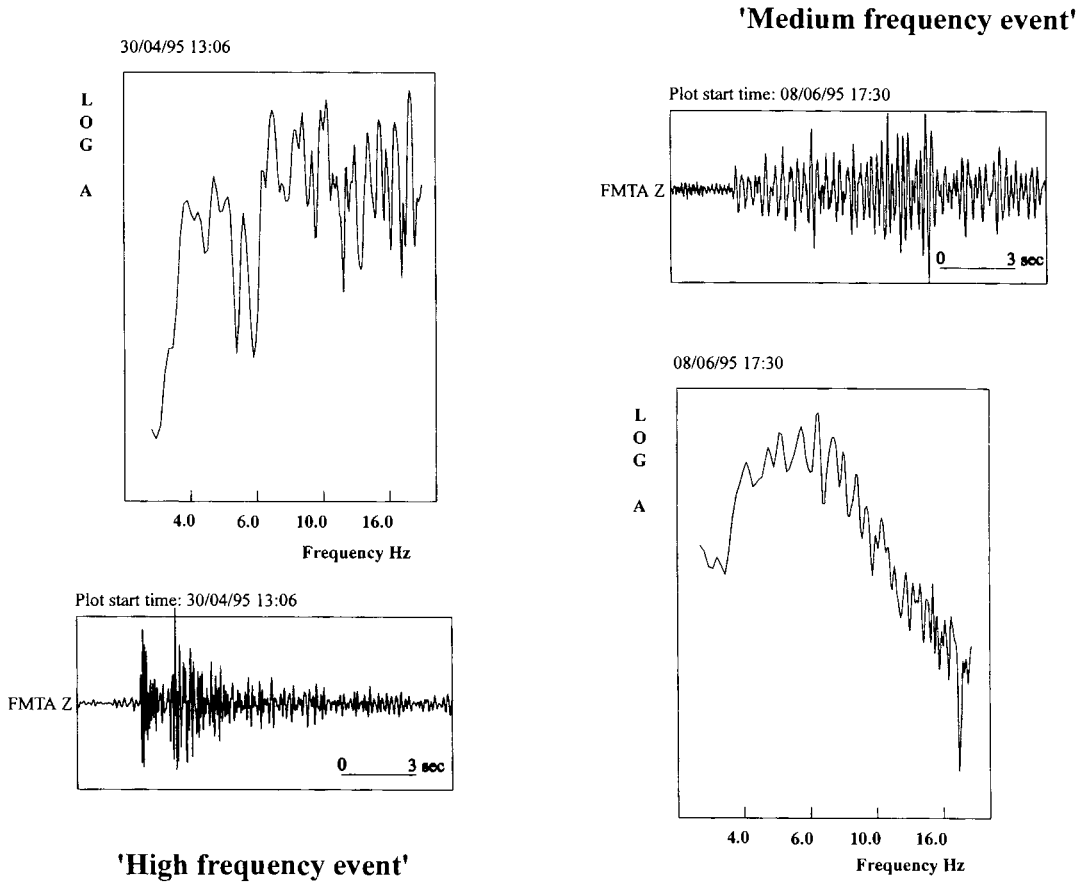

Fig. 4. Examples of vertical component velocity traces and frequency spectra of seismic events recorded during the 1995 Fogo eruption, one for each class discussed in the text.

ity. The lower level of seismic activity detected during this phase is not necessarily a real feature of the eruption, since the detection threshold was raised by the higher volcanic noise. Evidence for magma-drainback during the second phase comes from the occurrence of 45 min of strong volcanic tremor on May 30, followed by 36 h of swarm activity (close to 800 events, reaching a rate of one event per minute). The third phase lasted until the end of the monitoring.

Due to the total lack of information about the shallow velocity structure of Fogo island, a combination of two velocity models compiled by Brink and Brocher (1987), one for the Cape Verde Rise (offshore) and the other for the Canary Islands (onshore), were used for the hypocentral locations. The latter model was used for the upper 3.5 km of the crust. Only the solutions with rms residuals below 0.2 s and angular gaps up to 240° were retained. For 95% of the selected locations the rms residuals are less

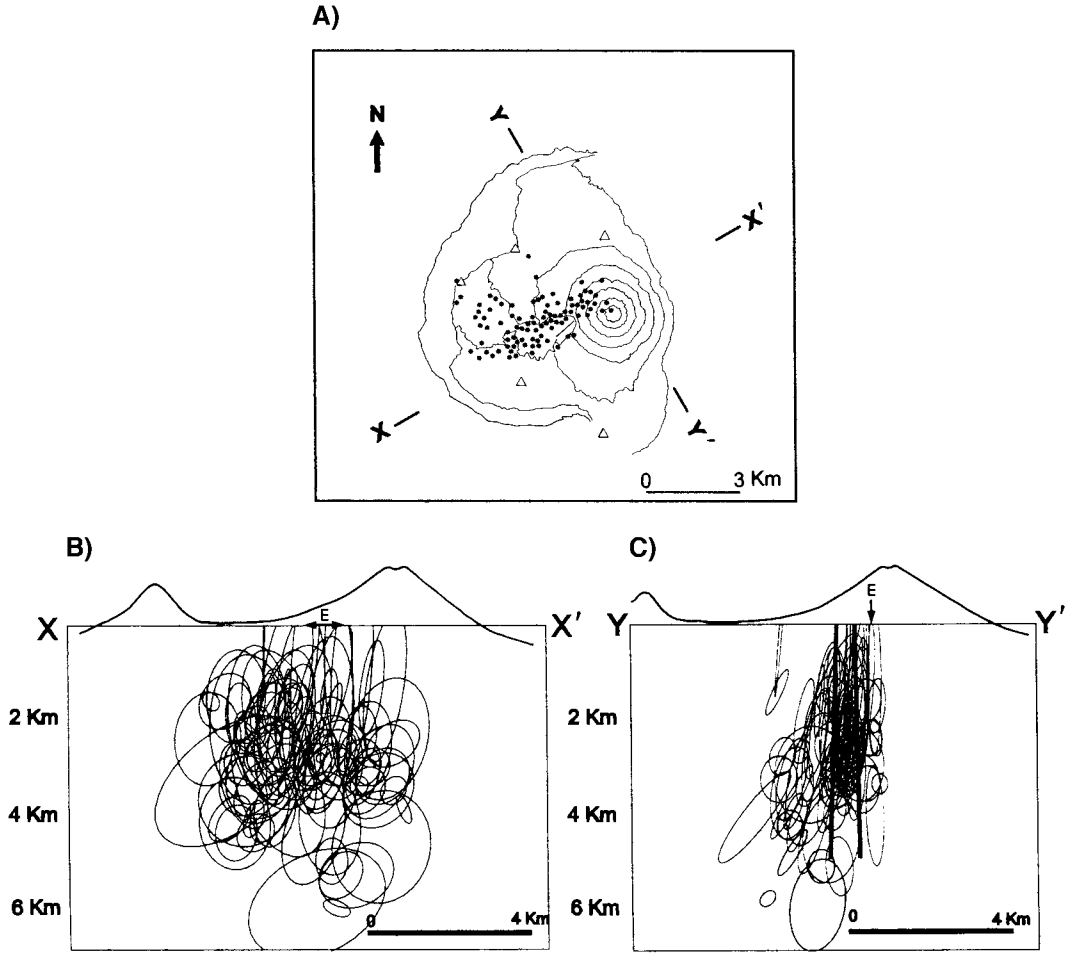

Fig. 5. (A) Epicentral distribution of the 'medium frequency' events. (B) Hypocentres of the 'medium frequency' events, projected in a section parallel to the surface fissure, showing the horizontal broadening of the inferred dyke at depths between 2 km and 4 km. The double arrow marked (E) shows the locus of the fissure. (C) Hypocentres of the 'medium frequency' events, projected on a section perpendicular to the surface fissure. The thick solid lines delimit the location of the interpreted dyke, and the arrow marked (E) shows the projection of the surface fissure. A possible NW dip of the dyke is suggested by the deeper hypocentres.

than 0.1 s, whereas for 50% of the hypocentres the angular gaps are below 180°. Fig. 3 shows the spatial distribution of the hypocentres and associated error ellipses.

The events were classed, according to their spectral content, as 'high frequency events' and 'medium frequency events' (Fig. 4). Using one of the stations as reference, a smoothed version of the velocity frequency spectrum was inspected and the ratio between the areas above 10 Hz and below 10 Hz was used as classification: 'high (medium) frequency events' have an areal ratio larger (smaller) than one. It should be noted that earthquakes usually classed as B-type or long-period (e.g., Minakami, 1974; Chouet, 1996), with typical frequencies in the range 0.5–5 Hz, will be cut-off by the sensors used in the present survey. In Figs. 5 and 6, the hypocentral distributions for 'medium frequency' and 'high frequency' events are shown separately.

Whenever the seismic signals showed clear onsets, a first-motion polarity was read and composite focal solutions were computed by trial-and-error, according to the following conditions: (1) events to be joined should be grouped in space and (2) should correspond to the same eruptive phase. Less clear but still readable polarities (mostly in connection with

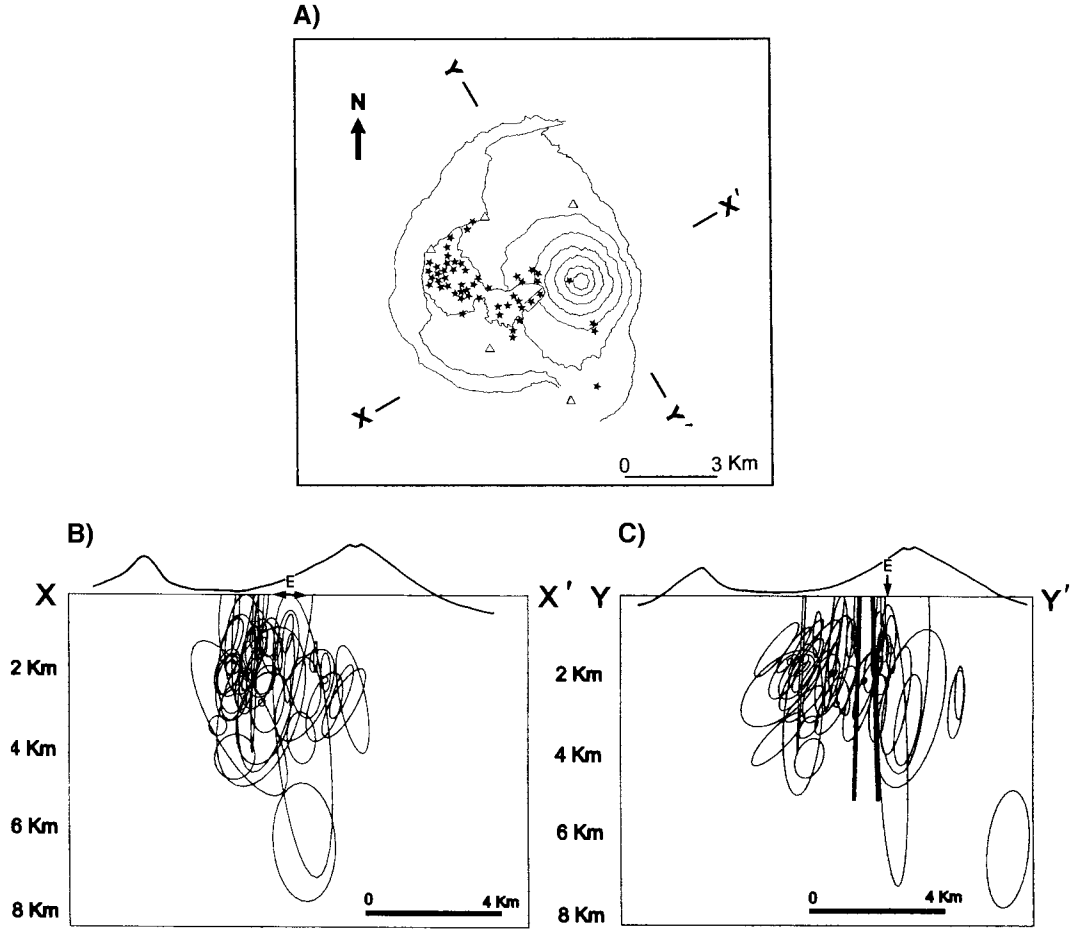

Fig. 6. (A) Epicentral distribution of the 'high frequency' events. (B) Hypocentres of the high-frequency events, projected in a section parallel to the surface fissure. (C) Hypocentres of the 'high frequency' events, projected on a section perpendicular to the surface fissure. See legend of Fig. 5 for a more detailed explanation of the symbols.

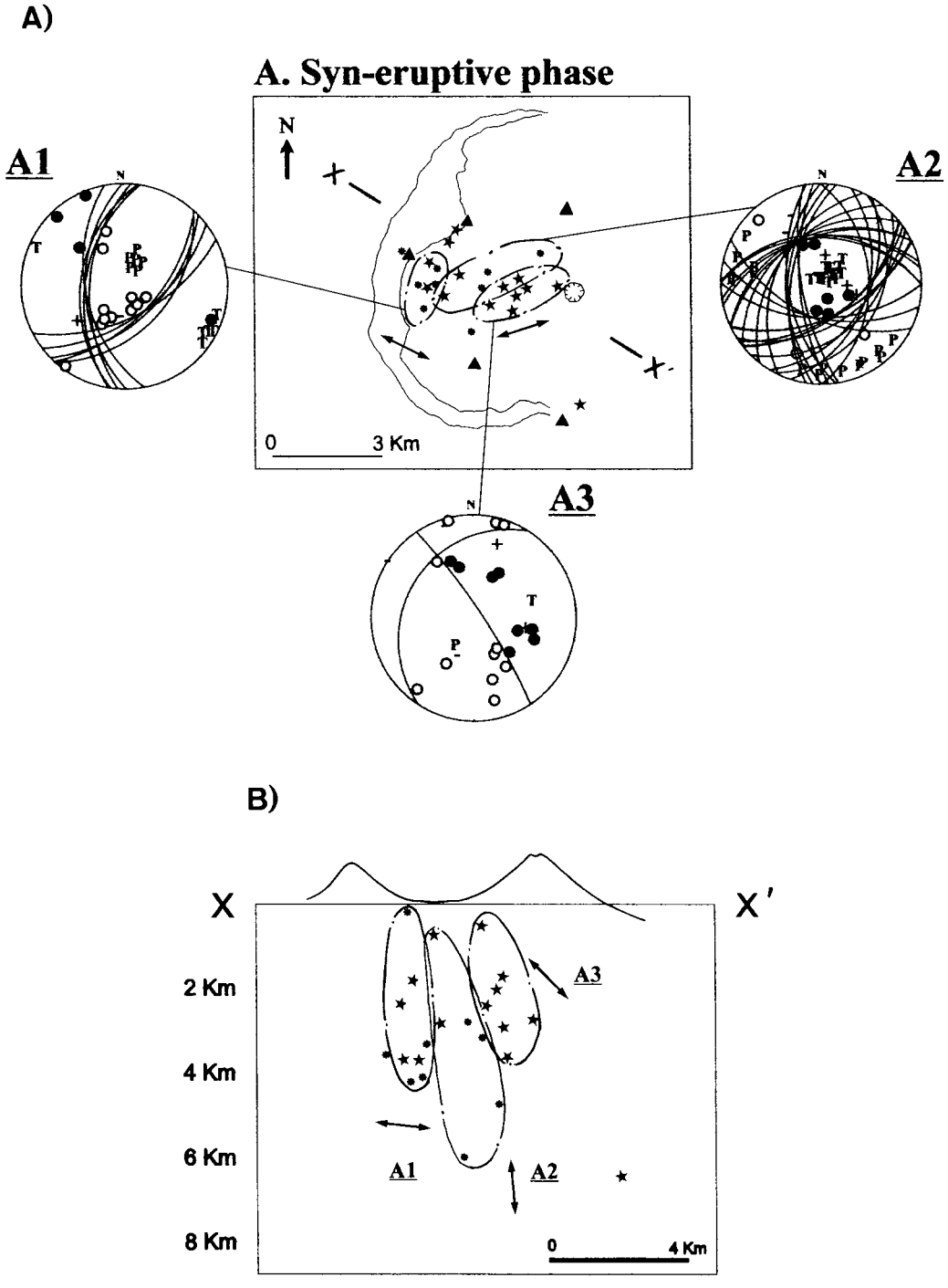

Fig. 7. (A) Composite focal mechanisms for the events of the syn-eruptive phase, in lower-hemisphere stereographic projection. All possible nodal planes found by an automatic search algorithm with 10° increments are displayed. Open (filled) circles show clear dilational (compressional) first motions, minus (plus) signs show less clear dilational (compressional) first motions. Asterisks are 'medium frequency' events, stars are 'high frequency' events. Double arrows show the projected directions of least compressive stress estimated from the focal mechanisms. (B) Hypocentres and estimated least compressive stress directions projected on section X–X′.

'medium frequency' events) were assigned a different symbol (see legend of Fig. 7). About 85% of the seismic events identified were not used in this first-motion study. Figs. 7–9 show the computed joint focal solutions for the syn-eruptive phase (groups A1 to A3), the drainback phase (groups B1 to B3) and

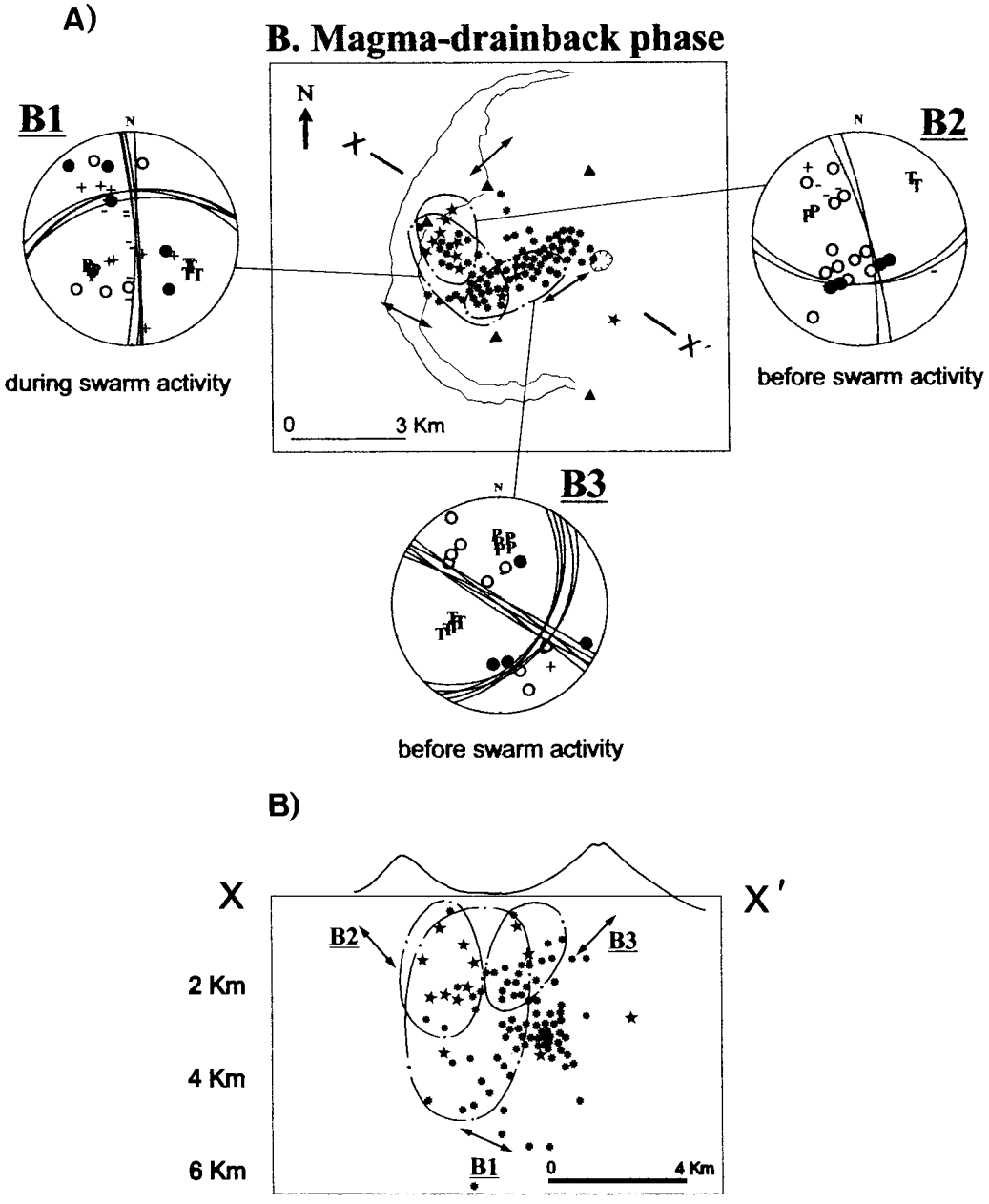

Fig. 8. (A) Composite focal mechanisms for the events of the magma-drainback phase, in lower-hemisphere stereographic projection. Events in overlapping clusters correspond to different intervals of time. See legend of Fig. 7 for details. (B) Hypocentres and estimated least compressive stress directions projected on section X–X′.

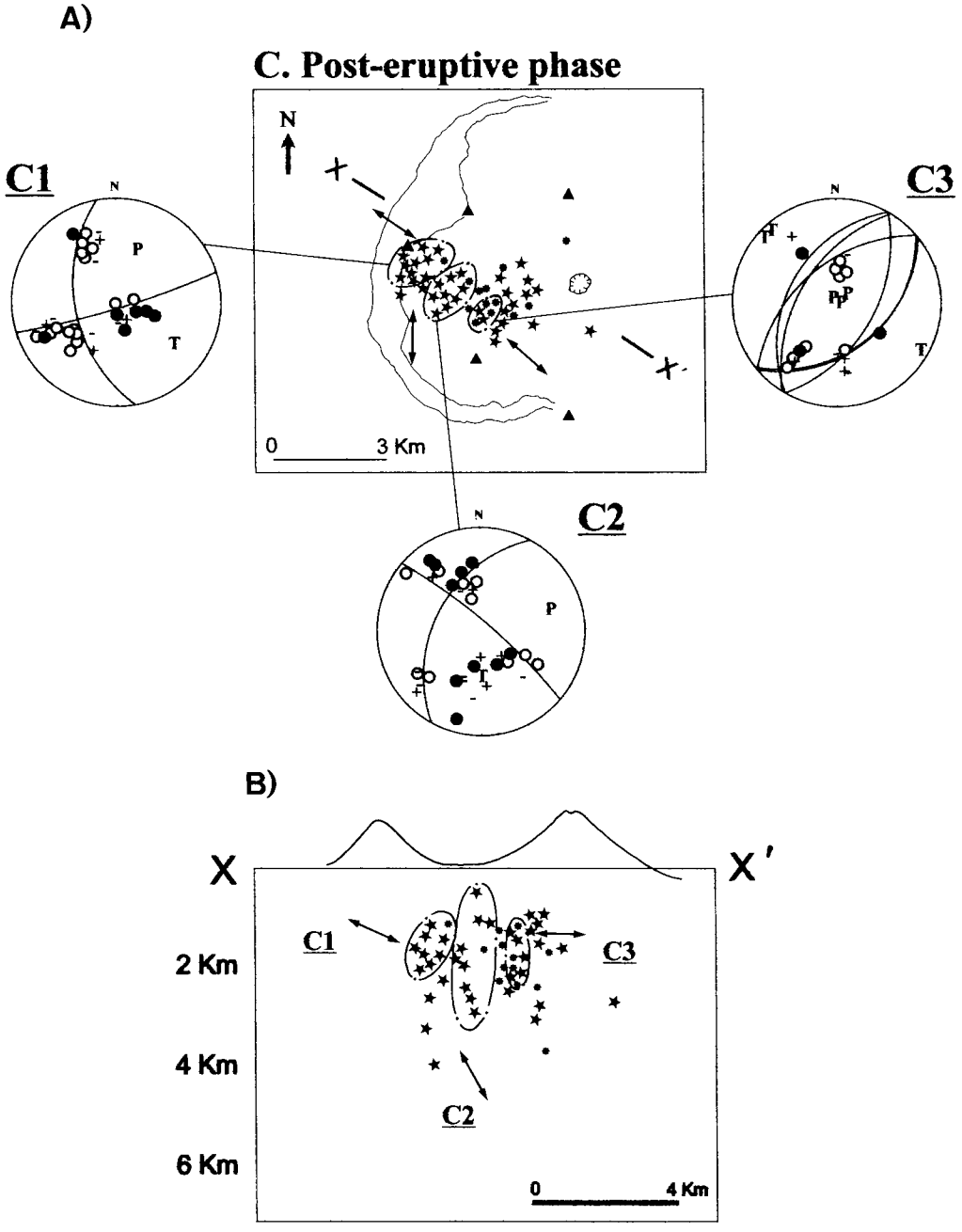

Fig. 9. (A) Composite focal mechanisms for the events of the post-eruptive phase, in lower-hemisphere stereographic projection. See legend of Fig. 7 for details. (B) Hypocentres and estimated least compressive stress directions projected on section X–X′.

the post-eruptive phase (groups C1 to C3), respectively. Fig. 10 shows, for all focal solutions, the directions of tension (T) axes, which will be considered as estimates of the directions of the minimum compressive stress σ_3. A group of T-axes is depicted in the NW–SE quadrants (solutions A1, B1, C1 and

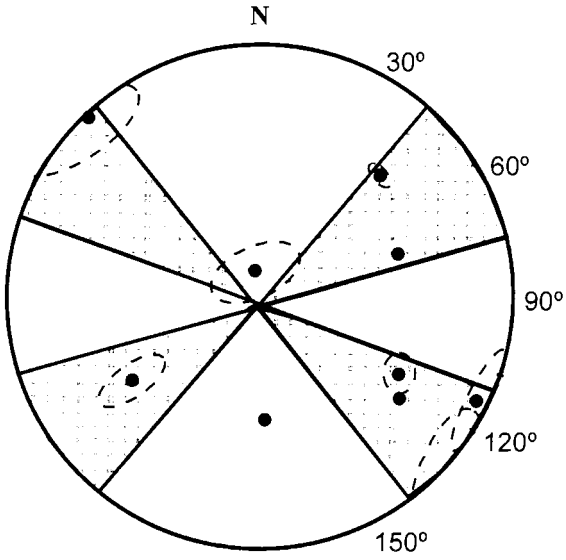

Fig. 10. Estimated tension axes for all the composite focal mechanisms in Figs. 7–9 (lower-hemisphere projections). The dashed contours delimit the scatter of possible axes.

C3) and a second group in the NE–SW quadrants (solutions A3, B2, and B3).

3. Discussion

3.1. Hypocentral distribution

As can be seen in Figs. 3, 5 and 6, the seismicity defines two trends, around 060° and around 120°. The 060° trend is dominated by 'medium frequency' events, and is particularly clear in the depth range of 0–4 km. It defines a nearly vertical zone underneath the eruptive fissure and with the same strike. We suggest that this 060° trend is the strike of a planar sub-vertical intrusion, which can be traced in Fig. 5C), and that its 'medium frequency' seismic activity is associated with failure of crustal material of reduced shear strength (Montalto, 1994). The thermally-induced increase of pore-fluid pressure occurring in the vicinity of the hot magma may be the cause of such change of the mechanical properties (Elsworth and Voight, 1996). The cross-section of this inferred dyke is nearly free from 'high frequency' events (Fig. 6C), and this is compatible with the above-comments.

Although the strike of the inferred intrusion is in good agreement with the orientation of the surface fissure, it is shifted about 400 m to the NW. This could result from the northwestward dip of the dyke suggested by Fig. 5C, but a systematic location error cannot be ruled out, due to the poor knowledge of the velocity model. The surface deflation pattern estimated from ERS-1 radar interferometry combining images of Fogo prior to and after the eruption (Amelung et al., 1997) is also in good agreement with the strike of the interpreted dyke (Fonseca et al., 1998).

Focal mechanism A2, computed for events of the syn-eruptive phase distributed along the 060° trend (see Fig. 7), shows a vertical *T* axis. This stress field can be predicted in the neighbourhood of a dyke that rises up to a shallow level, a situation in which the magma pressure is likely to exceed the maximum compressive stress in the host rock (Dahm and Brandsdóttir, 1997).

The 060° trend became clearer during the magma-drainback phase (Fig. 8), namely during the 36-h-long seismic swarm mentioned above. This may be the result of phreatomagmatic interaction between fluids entering the emptying feeder dyke and the top of the magma, inducing deformation of the host rocks (Delaney, 1982; Wohletz, 1986) and/or explosive processes (McNutt, 1986; Wohletz, 1986; Mori et al., 1989). The latter interpretation is supported by the fact that the events of the seismic swarm exhibit somewhat distinct signatures from the other 'medium frequency' events, with larger number of emergent onsets and less clear S arrivals. Also, due to the strong predominance of first-motion compressions, no double-couple focal solution could be fitted to this group of events, suggesting an explosive nature.

According to the data, no magma chamber exists above a depth of 4 km. This is in agreement with independent evidence from petrologic studies of Fogo lavas, which indicate that the magma is fed directly from the crust/mantle boundary (Mendes et al., 1996). It remains, however, to be explained why no significant seismicity was detected at deeper levels, as observed in other instances when the magma is fed directly from deep sources (Castellano et al., 1993). This apparent conflict may be solved by taking into account that the seismicity was not monitored during the pre-eruptive phase and the very

beginning of the eruption. The in-plane section of Fig. 5B shows that at depths between 2 km and 4 km, the intruding dyke reaches a maximum length of the order of 4 km, suggesting some amount of magma storage, possibly before the seismic monitoring.

The 'high frequency' seismicity is more developed during the post-eruptive phase (Fig. 9), and its interpretation is less straightforward because it does not follow the trend of the fissure. Instead, it shows an elongation trending at 120° (Fig. 6A), which does not correspond to a known structural trend.

It is interesting to note that the 120°-trending group of events correlates well with the area covered by the newly formed lava flows (Fig. 6A), and this could indicate that the deformation is induced by the new surface load. A similar effect is frequently observed following the impoundment of dam reservoirs, and is usually interpreted as indicative of self-organised criticality of the state of stress (Scholz, 1994).

3.2. Tension axis directions

In a homogenous isotropic material, newly formed failure allows a reliable estimate of the directions of principal stress. In the crust, however, failure occurs generally by reactivation of pre-existing planes of weakness, and if a few weak planes exist in a region, the choice of failure orientation is restricted. The only inference that can be made in this case is that the direction of σ_3 must be contained in the compressional quadrant of the focal mechanism (McKenzie, 1969). If a population of earthquakes in a region of uniform stress field has significantly different individual focal mechanisms, they should still be all compatible with the common stress tensor (Rivera and Cisternas, 1990). In a highly heterogeneous medium such as a volcano, it can be assumed that the distribution of potential planes of failure is widespread. In this case, the actual failure should not deviate strongly from the direction predicted for a homogeneous isotropic material (Célérier, 1988), and the scatter of the *P* and *T* axes (estimates of σ_1 and σ_3, respectively) is likely to be small.

The basic assumptions underlying the estimates of σ_3 directions presented here are that (1) a group of events corresponding to the same region and to the same phase of the eruption occur under the same stress field and (2) while the nodal planes cannot be resolved for each individual event and may differ significantly, the directions of principal stress can still be estimated using the joint focal mechanism that best fits the population of observed first-motion polarities. The non-uniqueness of single-event solutions will generate considerable uncertainty on the inferred tension axis directions (Jupe, 1993), and the results presented here must therefore be regarded as general indicators of the true directions of minimum compressive stress.

The intrusion of a dyke requires the least compressive stress direction to be perpendicular to its strike (e.g., Nakamura, 1977). For the inferred dyke, one of the groups in Fig. 10 (NW–SE tension axes) verifies this condition satisfactorily, at least in horizontal projection, and therefore seems to have a causal link with the occurrence of the eruption. This type of *T* axis orientation can be seen towards the NW of the dyke during the syn-eruptive phase (A1), the swarm activity (B1), and at shallow depths in the post-eruptive phase (C1 and C3). Towards the SE side of the dyke, however, this direction of tension axes is not detected. The possible dip of the dyke towards the NW discussed in Section 3.1 would account for this asymmetry (Pollard et al., 1983).

The 060° trend of the 1995 intrusion coincides with the orientation of one of the rift zones described in Section 1, and is close to perpendicular to the NW–SE tension axes of Fig. 10. The development of this stress field may therefore signal a reactivation of the WSW rift zone after at least several centuries of inactivity. This inference is supported by the results obtained by the deployment of a temporary seismic network in early 1994 (Heleno da Silva and Fonseca, in press). This network recorded seismic unrest along the strike of this rift zone, in the direction of the adjacent island of Brava, and at some 40 km distance from the site of the 1995 eruption.

The group of tension axes in the NE–SW quadrants (Fig. 10), i.e., nearly parallel to the trend of the dyke, is not directly related to the driving mechanism of the intrusion. A possible explanation for this seismicity is the re-adjustment to the new conditions inside the volcanic edifice. Since the Cape Verde Rise is a quiet tectonic environment (Wysession et al., 1995), local stresses related to topography or magmatic processes are likely to constrain this re-ad-

justments more effectively than stresses of plate tectonic origin. At a more local scale, pre-existent structures such as the buried collapse scar (Day et al., 1999-this volume) may have been reactivated during these re-adjustments, but the data are also compatible with a more random redistribution of stresses in the heterogeneous edifice.

During the magma drainback phase, the tension axis underneath Pico do Fogo rotates, dipping now towards the W (Fig. 8B), and the corresponding focal solution B3 becomes compatible with predominantly dip-slip motion on a plane dipping towards the East. This plane may correspond to detachment surfaces, distributed between 1 km and 2.5 km of depth (i.e., the depth range of the seismicity cluster), on which parts of the eastern flank of the island within the Monte Amarelo collapse scar have moved towards the sea. A similar effect was proposed to explain the shallow (less than 2 km deep) seismicity observed in the eastern flank of Etna by Montalto et al. (1996) and attributed to gravitational sliding.

The rotation of the minimum compressive stress underneath Pico do Fogo during the magma-drainback phase, and the associated decrease of flank stability, could be due to a reduction of friction on the assumed detachment surface due to pore fluid pressurisation (Elsworth and Voight, 1995). The timing of the estimated change in the stress field, after the end of the eruption, favours also the control of thermal pressurisation of pore fluids on the shear strength of the edifice (Elsworth and Day, 1999-this volume).

4. Conclusions

The seismic monitoring allowed the identification of a planar sub-vertical intrusion, with horizontal length of at least 4 km and a strike of 060°, as the cause of the April 1995 Fogo eruption. A swarm of seismic events immediately after the end of the effusive phase, possibly due to interaction between phreatic fluids and the retreating magma, was particularly effective in delineating this intrusion at depth.

The strike of the intruding dyke contrasts with the geometry of historical eruptions during the last 250 years, which occurred on N–S fissures apparently associated with E–W gravity-driven extension. On the other hand, the current trend suggests the re-use of an older preferential direction of rifting, inferred from geological observations.

The directions of least compressive stress estimated from several joint focal mechanisms are nearly at right angles with the orientation of the dyke, as would be expected. However, a significant part of the recorded deformation seems to deviate strongly from this rule, suggesting a re-adjustment to the new state of stress in which gravity may have played an important role. The steep eastern flank of the island may have been destabilised by this effect, since during the magma drainback, the deformation is compatible with predominantly dip-slip motion on east-dipping detachment surfaces.

Gravitational instability of the eastern flank of Fogo Island during and after future eruptions is a major volcanic hazard, since it could lead to a large-scale lateral collapse (Day et al., 1999-this volume). The effect of eruptive processes on the stability and collapse potential of the active volcano on Fogo deserves further investigation.

Acknowledgements

The authors thank BGS, UK for the loan of the seismographic equipment, and in particular Mr. D. Stewart and Ms. A. Walker for their support. Fieldwork in Fogo was funded by the EU (contract ECHO/TPS/B7-219/95/0101), JNICT, Lisbon, and ICP, Lisbon. Logistic support was provided by Mosteiros City Council, Fogo, and the Ministry of Defense of Cape Verde. An earlier version of this manuscript was improved by the comments of two anonymous reviewers. One of the authors (SINH) holds a research studentship from Programme PRAXIS XXI, Lisbon. The Gulbenkian Foundation, Lisbon, supported the fieldwork of one of the authors (SJD).

References

Amelung, F., Zebcker, H., Segall, P., 1997. Surface deformation measurements of volcanoes using SAR interferometry (abstract). EOS AGU Trans. 46, F818, Supplement.

Brink, U.S.T., Brocher, T.M., 1987. Multichannel seismic evidence for a subcrustal intrusive complex under Oahu and a model for Hawaiian volcanism. J. Geophys. Res. 92, 13687–13707.

Carracedo, J.C., 1994. The Canary islands: an example of structural control on the growth of large oceanic-island volcanoes. J. Volcanol. Geotherm. Res. 60, 225–241.

Carracedo, J.C., 1999. Growth, structure, instability and collapse of Canarian volcanoes and comparisons with Hawaiian islands. J. Volcanol. Geotherm. Res. 94, 1–19.

Castellano, M., Ferruci, F., Godano, C., Imposa, S., Milano, M., 1993. Upwards migration of seismic focii: a forerunner of the 1989 eruption of Mt. Etna (Italy). Bull. Volcanol. 55, 357–361.

Célérier, B., 1988. How much does slip on a reactivated fault plane constrain the stress tensor? Tectonics 7 (6), 1257–1278.

Chouet, B.A., 1996. Long-period volcano seismicity: its source and use in eruption forecasting. Nature 380, 309–315.

Dahm, T., Brandsdóttir, B., 1997. Moment tensors of microearthquakes from the Eyjafjallajökull volcano in South Iceland. Geophys. J. Int. 130, 183–192.

Day, S.J., Heleno da Silva, S.I.N., Fonseca, J.F.B.D., 1999. A past giant lateral collapse and present-day flank instability of Fogo, Cape Verde islands. J. Volcanol. Geotherm. Res. 94, 191–218.

Delaney, P.T., 1982. Rapid intrusion of magma into wet rock: groundwater flow due to pore pressure increases. J. Geophys. Res. 87 (B9), 7739–7756.

Elsworth, D., Day, S.J., 1999. Flank collapse triggered by intrusion: the Canarian and Cape Verde archipelagos. J. Volcanol. Geotherm. Res. 94, 323–340.

Elsworth, D., Voight, B., 1995. Dike intrusion as a trigger for large earthquakes and the failure of volcano flanks. J. Geophys. Res. 100, 6005–6024.

Elsworth, D., Voight, B., 1996. Evaluation of volcano flank instability triggered by dyke intrusion. In: McGuire, W.J., Jones, A.P., Neuberg, J. (Eds.), Volcano Instability on the Earth and other Planets. Geol. Soc. London, Spec. Publ., Vol. 110, pp. 125–135.

Fonseca, J.F.B.D., Heleno da Silva, S.I.N., Walker, A.B., Barros, I.J., Quental, L.M.A.R., Stewart, D., Ramos, M.M., 1996. Seismic monitoring of the Fogo eruption, April 95. In: Thorkelson, B. (Ed.), Seismology in Europe. IMO, Reykjavik, 1996.

Fonseca, J.F.B.D., Day, S.J., Matos, J.L.G., Lima, J.N.P., Berberan, A., Heleno da Silva, S.I.N., Amelung, F., d'Oreye, N., 1998. Ground deformation monitoring in the Fogo Volcano, Cape Verde Islands. Comptes Rendus of the 83rd Journées Luxembourgeoises de Géodynamique. ECGS, Luxembourg.

Gaspar, J.L., Wallenstein, N., Queiroz, G., Ferreira, T., Coutinho, R., Gomes, A., 1995. Resumo da actividade vulcânica registada na Ilha do Fogo (Cabo Verde) nos meses de Abril e Maio de 1995. In: Borges, F., Marques, M. (Eds.), Resumos alargados do 4° Congresso Nacional de Geologia. Universidade do Porto.

Global Volcanism Network Bulletin, 1995. 20 (3) 2–4.

Heleno da Silva, S.I.N., Fonseca, J.F.B.D., in press. A seismological investigation of Fogo Volcano, Cape Verde Islands: preliminary results. Volcanology and Seismology, 1.

Jupe, A., 1993. How well are principal stress axes constrained by non-unique fault-plane solution data? Geophys. J. Int. 115, 319–322.

Lienert, B.R., 1994. HYPOCENTER 3.2 Manual. HIGP, Honolulu.

McKenzie, D.P., 1969. The relation between fault plane solutions for earthquakes and the directions of the principal stresses. Bull. Seismol. Soc. Am. 59 (2), 591–601.

McNutt, S.R., 1986. Observations and analysis of B-type earthquakes, explosions, and volcanic tremor at Pavlof volcano, Alaska. Bull. Seismol. Soc. Am. 76 (1), 153–175.

Mendes, M.H., Munhá, J., Palácios, T., Silva, L.C., Torres, P.C., 1996. Petrology and Geochemistry of 1995 and other historic eruptions from Fogo Island (Cape Verde). Abstracts of the International Congress on the Volcanic Eruption of 1995 in Fogo Island, Cape Verde. IICT, Lisbon.

Minakami, T., 1974. Seismology of volcanoes in Japan. In: Civetta, L., Gasparini, P., Luongo, G., Rapolla, A. (Eds.), Physical Volcanology. Elsevier, Amsterdam, pp. 1–27.

Montalto, A., 1994. Seismic events at Vulcano (Italy) during 1988–1992. J. Volcanol. Geotherm. Res. 60, 193–206.

Montalto, A., Vinciguerra, S., Menza, S., Patanè, 1996. Recent seismicity of Mount Etna: implications for flank instability. In: McGuire, W.J., Jones, A.P., Neuberg, J. (Eds.), Volcano Instability on the Earth and Other Planets. Geol. Soc. London, Spec. Publ., Vol. 110, pp. 169–177.

Mori, J., Patia, H., McKee, C., Itikarai, I., Lowenstein, P., De Saint Ours, P., Talai, B., 1989. Seismicity associated with eruptive activity at Langila Volcano, Papua New Guinea. J. Volcanol. Geotherm. Res. 38, 243–255.

Nakamura, K., 1977. Volcanoes as possible indicators of stress orientation: principle and proposal. J. Volcanol. Geotherm. Res. 2, 1–16.

Pollard, D.A., Delaney, P.T., Duffield, W.A., Endo, E.T., Okamura, A.T., 1983. Surface deformation on volcanic rift zones. Tectonophysics 94, 541–584.

Ribeiro, O., 1960. A Ilha do Fogo e as suas Erupções, Junta de Investigação do Ultramar, Lisbon.

Rivera, L., Cisternas, A., 1990. Stress tensor and fault plane solutions for a population of earthquakes. Bull. Seismol. Soc. Am. 80 (3), 600–614.

Scholz, C.H., 1994. The Mechanics of Earthquakes and Faulting. Cambridge Univ. Press, p. 439.

Torres, P.C., Silva, L.C., Gomes, A.M., 1995. Geologia e vulcanologia da erupção de 1995 na Ilha do Fogo — Arquipélago de Cabo Verde — e formações enquadrantes. In: Borges, F., Marques, M. (Eds.), Resumos alargados do 4° Congresso Nacional de Geologia. Universidade do Porto.

Torres, P.C., Madeira, J., Silva, L.C., Brum da Silveira, A., Serralheiro, A., Mota Gomes, A., 1997. Carta geológica da Ilha do Fogo — Erupções históricas e formações encaixantes. Proceedings of the International Congress on the Volcanic Eruption of 1995 in Fogo Island, Cape Verde. IICT, Lisbon.

Wohletz, K.H., 1986. Explosive magma–water interactions: thermodynamics, explosion mechanisms and field studies. Bull. Volcanol. 48, 245–264.

Wysession, M.E., Wilson, J., Bartkó, L., Sakata, R., 1995. Intraplate Seismicity in the Atlantic Ocean Basin: a Teleseismic Catalog. Bull. Seismol. Soc. Am. 85 (3), 755–774.